Experimental Validation of a Deployment Mechanism for Tape-tethered Satellites

Andrea Valmorbida
Dept. Industrial Engineering
University of Padova
Padova, Italy
andrea.valmorbida@unipd.it

Lorenzo Olivieri
CISAS[1] "G. Colombo"
University of Padova
Padova, Italy
lorenzo.olivieri@unipd.it

Giulia Sarego
CISAS[1] "G. Colombo"
University of Padova
Padova, Italy
giulia.sarego@unipd.it

Alice Brunello
CISAS[1] "G. Colombo"
University of Padova
Padova, Italy
alice.brunello.3@phd.unipd.it

Davide Vertuani
CISAS[1] "G. Colombo"
University of Padova
Padova, Italy
davide.vertuani@studenti.unipd.it

Carlo Bettanini
Dept. Industrial Engineering
University of Padova
Padova, Italy
carlo.bettanini@unipd.it

Marco Pertile
Dept. Industrial Engineering
University of Padova
Padova, Italy
marco.pertile@unipd.it

Enrico C. Lorenzini
Dept. Industrial Engineering
University of Padova
Padova, Italy
enrico.lorenzini@unipd.it

***Abstract*—The number of space debris orbiting our Earth has been continuously increasing since the beginning of the space era. The space community is converging on responsible conducts and self-regulations to address this serious problem that is degrading the near-Earth environment. In this context, green deorbiting technologies and strategies alternative to the traditional chemical propulsion are under investigation, including Electrodynamic Tethers (EDTs) because they are a promising option. To increase EDT technology maturity level, some critical points shall be addressed and experimentally evaluated, including the deployment of tape tethers, to demonstrate their reliability. This paper presents results of an experimental validation of the Deployment Mechanism (DM) proposed for the H2020 FET OPEN Project E.T.PACK – Electrodynamic Tether Technology for Passive Consumable-less Deorbit Kit. We developed a mock-up that hosts the DM and other elements that are on board the tip mass of a tethered system, using off-the-shelf components. The DM is tested for the first part of the tether deployment maneuver employing the SPARTANS facility of the University of Padova. This facility includes a Testing Table where the mock-up can move with almost no friction and a Motion Capture system that provides an accurate estimation of the mock-up motion during this first part of the tether deployment maneuver.**

***Index Terms*—Deployment Mechanism for tape tether, Electrodynamic Tether (EDT), experimental validation, Motion Capture system.**

I. Introduction

Space tethers have been studied for several decades and may be employed for a wide range of applications [1], such as the study of plasma physics in the upper atmosphere [2], the orbit maintenance or deorbit of space vehicles [3], the orbital transfer of payloads employing motorised momentum exchange tethers [4], space tugging [5], space elevators [6] and even asteroid deflection [7]. More specifically for deorbiting purposes, space tethers appear to be a promising technology that overcome the limitations of traditional chemical and electric propulsion, that may be affected by propellant leakage or degradation in case of long storage time, and attitude control demands during disposal manoeuvres. Challenging and interesting aspects related to successful space tether missions are the deployer mechanism and the deployment control. Tether dynamics is highly nonlinear [8] and needs to be carefully studied for an accurate design of the deployer mechanism and the control of deployment dynamics [9]. Several issues have to be taken into consideration, such as the libration stability during deployment [10]–[12] and the definition of an ejection system required for the initial deployment of the tether.

Because of the complexity of a tethered system, its experimental validation is of significant value [13] to estimate key parameters affecting its dynamics and control during the deployment phase. The aim of this paper is to validate experimentally the functionality of a Deployment Mechanism (DM) developed within the framework of the H2020 FET OPEN Project E.T.PACK – Electrodynamic Tether Technology for Passive Consumable-less Deorbit Kit - and to assess the accuracy in tracking the reference deployment trajectories.

The work is organized as follows. Section II gives an overview of tether deployer, while section III describes the ground-based experimental setup. Section IV summarizes the results of numerical simulations while section V shows the experimental results.

II. Tether Deployer General Issues

One of the most challenging operations with tethers is the deployment phase. In the most common approach, the process starts with the release of a tethered tip mass from the host spacecraft (e.g. [14]). In close proximity, the gravity gradient forces acting on the system are negligible and consequently the tip mass is given an initial momentum to start tether deployment. Once few hundreds of meters are deployed, the gravity gradient becomes the leading driver in the deployment

[1]Center of Studies and Activities for Space "Giuseppe Colombo" (CISAS)

process.

The whole operation requires a continuous control of the tip mass trajectory, because an uncontrolled deployments may result in large libration oscillations that can lead to unstable conditions (e.g. system turning upside down). Specifically, with oscillations above 65 deg the tether looses tension [15] during parts of the libration cycle, a condition that is not desirable from the overall stability point of view.

Reference deployment trajectories can be derived through an optimization process to provide stability (i.e. small libration oscillations) at the end of deployment. Such trajectories require optimal values of the tip mass initial ejection direction and momentum and provide the reference profile of tether deployment velocity vs time that shall be controlled by the deployment mechanism. The deployer ability to follow predefined deployment profiles is therefore fundamental to have a desirable deployment procedure; design considerations shall be supported by subsystem and system verification in a relevant environment.

Passive (internal friction) and active control systems (e.g. active motor control) can be employed to control deployment. To provide the initial momentum to the tip mass, mechanical springs [16], electro-mechanical deployable masts [17] or propulsive cold gas thrusters [18] have been proposed. Different deployment mechanisms have been designed, depending on the deployment strategy. They can be classified in three main categories: rotating reels, stationary spools, and folded "origami" tethers; the latter solution is usually preferred for short tethers.

In the framework of the E.T.PACK project, a deployer kit prototype is currently under development to deploy up to a three-kilometer long tape tether [19]. The kit is designed to act as tip mass and to provide the initial momentum thanks to a small propulsive unit (cold gas actuator). A sketch of the kit can be seen in Fig. 1.

The kit capability to deploy the tether is assessed with a laboratory campaign of experiments on a low-friction table, employing a scaled model of the E.T.PACK tip mass, as described in the following sections.

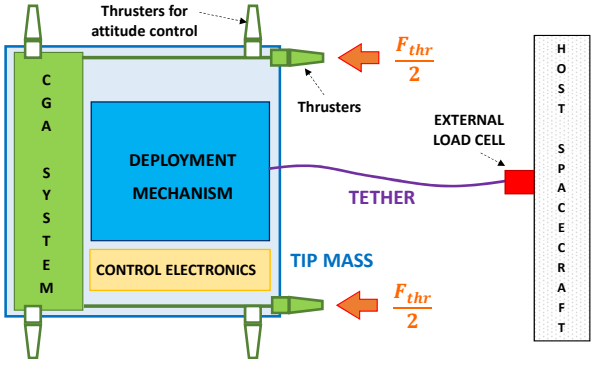

Fig. 1. E.T.PACK kit sketch: the tip mass includes the tether deployment mechanism with the tether reel, the control electronics and the Cold Gas Assembly (CGA) system with tank and nozzles.

III. Ground-based Experimental Setup

To validate the Deployment Mechanism for tape-shaped tethers, we developed a tip mass mock-up with the tether deployment system placed on board an air carriage that includes three air bearings on its bottom part for a low-friction motion on a flat surface. Specifically, the tip mass mock-up includes: a) a tether reel with $30\,m$ of an Aluminium tape tether; b) an actuated deployment mechanism equipped with a motor and a series of pulleys; c) a passive brake coupled to the reel; d) a Cold Gas Assembly (CGA) system; and e) the command and control electronics. A picture of the kit mock-up can be seen in Fig. 2. Figure 3 shows a sketch of the deployment mechanism with its main components and the internal sensors and actuators.

The experiment is being carried out with the SPARTANS facility of the University of Padova [20]–[22], that includes a $2\,m$ by $3\,m$ Testing Table, over which the tip mass mock-up can move at very-low friction, and a Motion Capture (MC) system with 6 infra-red cameras with acquisition frequency of $50\,Hz$ to track the motion of retro-reflective spherical markers moving within their operative volume. Specifically, each retro-reflective spherical marker is tracked with a sub-millimeter accuracy in position. In addition, using 3 retro-reflective spherical markers on-board the mock-up with a baseline of $\sim 0.5\,m$, the MC system can provide an estimation of the mock-up attitude with an accuracy of $0.1\,deg$ [23].

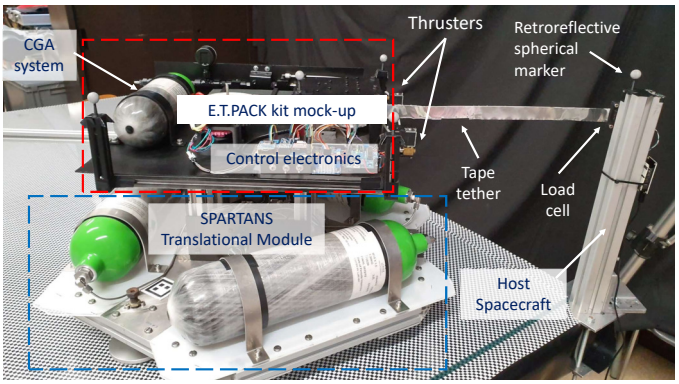

Fig. 2. E.T.PACK kit mock-up with the main components integrated on the translational module of the SPARTANS facility.

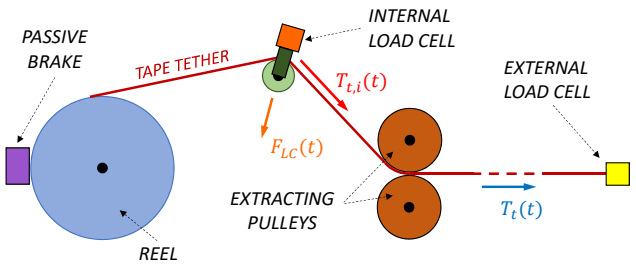

Fig. 3. Sketch of the deployment mechanism.

The retro-reflective spherical markers are employed to track some specific points on both the tip mass and the host spacecraft and define the Reference Frames (RFs) used during the experimental validation of the deployment mechanism [23], as described in the following section III-A.

A. Reference Frames

Referring to Fig. 4, the following RFs are defined.

a) Global Reference Frame G: The external Global RF is a Local Vertical - Local Horizontal (LV-LH) frame of reference defined during the initialization procedure of the Motion Capture System. The estimated positions of all the retro-reflective markers used during the experiment are expressed in this frame of reference.

b) Body Reference Frame B of the tip mass mock-up: This RF is defined by a set of 3 retro-reflective markers M_0, M_1 and M_2 placed at the three top vertices of the mock-up. First, the two unit vectors $\widehat{\mathbf{p}}$ and $\widehat{\mathbf{q}}$ are defined:

$$\widehat{\mathbf{p}} = \frac{\mathbf{M}_1 - \mathbf{M}_0}{\|\mathbf{M}_1 - \mathbf{M}_0\|_2} \tag{1}$$

$$\widehat{\mathbf{q}} = \frac{\mathbf{M}_2 - \mathbf{M}_0}{\|\mathbf{M}_2 - \mathbf{M}_0\|_2} \tag{2}$$

where $\mathbf{M}_i$ is the 3D position of the markers M_i expressed in the Global RF. After that, the axes of the Body RF are defined as $\mathbf{X}_B = \widehat{\mathbf{p}}$, $\mathbf{Z}_B = \widehat{\mathbf{p}} \times \widehat{\mathbf{q}} / \|\widehat{\mathbf{p}} \times \widehat{\mathbf{q}}\|$ and $\mathbf{Y}_B = \mathbf{Z}_B \times \mathbf{X}_B$. The origin of this frame of reference $\mathbf{O}_B$ is located at the geometric center of the E.T.Pack kit mock-up. The estimation of the markers M_0, M_1 and M_2 positions, provided by the MC system, allows to compute the roto-translation matrix from RF B to RF G ${}^G_B\mathbf{T} = [{}^G\mathbf{t}_B, {}^G_B\mathbf{R}]$.

c) Body Reference Frame A of the host satellite: This RF represents the Body RF of the host spacecraft and is defined by a set of 3 retro-reflective markers M_3 M_4 and M_5 placed on the fixed anchoring structure for the tether, similarly to the definition of the mock-up Body RF. The roto-translation matrix from RF A to RF G ${}^G_A\mathbf{T} = [{}^G\mathbf{t}_A, {}^G_A\mathbf{R}]$ is computed employing the positions of the retro-reflective markers M_3 M_4 and M_5 estimated by the MC system.

B. Experimental procedure

The objective of this work is to demonstrate that the Deployment Mechanism is able to operate properly during the early and critical part of the tether deployment meeting the following two requirements:

1) RQ1 – the actual tether length $l(t)$ and length rate $\dot{l}(t)$ have to follow the corresponding precomputed reference trajectory $l_{ref}(t)$ and $\dot{l}_{ref}(t)$;
2) RQ2 – the oscillation of the tip mass mock-up about the tether direction have to be within $\pm 10\,deg$ in amplitude, so that the CGA thrust direction is mainly aligned with the tether direction.

To estimate the actual tether length $l(t)$ and length rate $\dot{l}(t)$ needed to verify the requirement RQ1, we employed two retro-reflective markers in addition to the six ones employed to define the frames of reference A and B (see Fig. 4): (1) the first one M_6 is placed on the tip mass in correspondence of the exiting point of the tether from the tip mass; and (2) the second one M_7 is placed on the host spacecraft in correspondence of the anchoring point of the tether to the fixed external structure. The MC system provides an estimation of the 3D position of the retro-reflective markers M_6 and M_7 expressed in the Global RF and at each acquisition time t_k, i.e. $\mathbf{M}_6(t_k)$ and $\mathbf{M}_7(t_k)$ respectively. The tether length can be computed as $l(t_k) = ||\mathbf{M}_7(t_k) - \mathbf{M}_6(t_k)||_2$, while the tether length rate $\dot{l}(t_k)$ is computed as the first time derivative of the interpolating smoothing spline of $l(t_k)$.

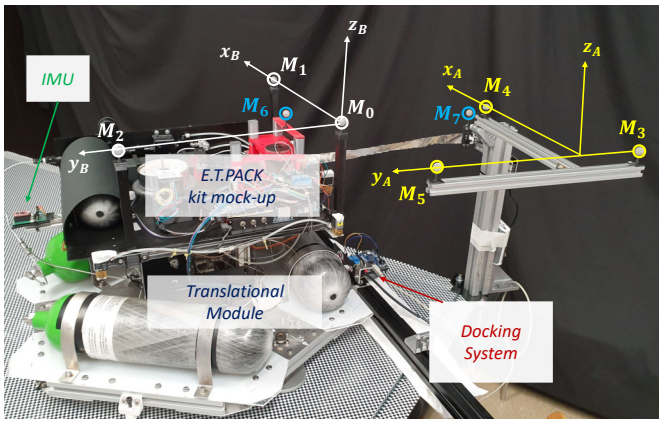

Fig. 4. Position of the Motion Capture retro-reflective markers on the E.T.PACK kit mock-up and definition of Reference Frames (RF's) axes orientation. The RF B is depicted in white and the RF A is depicted in yellow.

To verify the requirement RQ2, we need to monitor the actual relative position and orientation of the RF B with respect to the RF A, i.e. ${}^A\mathbf{t}_B(t)$ and ${}^A_B\mathbf{R}(t)$. From the estimations of the 3D positions of the retro-reflective markers with ID from 0 to 5 provided by the MC system, the roto-translation matrices ${}^G_B\mathbf{T}$ and ${}^G_A\mathbf{T}$ are computed as previously described. The relative position and orientation of the RF B with respect to the RF A can be retrieved by properly multiplying the two roto-translation matrices ${}^G_A\mathbf{T}$ and ${}^G_B\mathbf{T}$: ${}^A_B\mathbf{T} = [{}^A\mathbf{t}_B, {}^A_B\mathbf{R}] = {}^G_A\mathbf{T}^{-1} \cdot {}^G_B\mathbf{T}$.

Another goal during deployment is that the tape tether remains on average in tension on two portions (see also Fig. 3): (a) the tether portion between the host spacecraft and the tip mass, and (b) the tether portion internal to the deployment mechanism on board the tip mass. To this aim, two calibrated beam-type load cells were used. Specifically, a first load cell was placed at the interface between the tape tether and the host spacecraft to measure directly the tension of the tether during deployment $T_t(t)$ and therefore to verify that, with the imposed tether deployment profile, the tape does not experience high tension peaks or too long periods of slackness. In addition, we used a second load cell internal to the deployment mechanism to monitor the tension of the tape $T_{t,i}(t)$ between the reel and the extracting pulleys.

We also employed a docking system based on electro-magnets in order to: (a) maintain the mock-up in a fixed

position before its release at the beginning of the deployment maneuver; and (b) to carry out multiple experimental tests with the mock-up having the same starting position and orientation.

The use of an active attitude control on the tip mass is required since the rotation of the tether reel induces a rotation of the tip mass in the opposite direction due to conservation of the Angular Momentum. The attitude control in the mock-up is implemented using 4 thrusters actuated in pairs to generate a net control torque about the vertical axis (see Fig. 2). In addition, the MC data are used as fiducial reference and are not transmitted in real-time to the mock-up on-board computer. To estimate and control the attitude of the mock-up during the deployment, an Inertial Measurement Unit (IMU) on-board the mock-up was used to feed a Proportional-Derivative (PD) control algorithm. The control torque computed by the PD algorithm is then actuated by modulating the time-width of the pulses of the attitude thrusters.

IV. Dynamic Simulations

The reference profiles for the deployment maneuver were obtained using the BOCOP software [24] to solve a boundary value problem: to find the time profiles of the control tether tension $T_p(t)$, the tether length $l(t)$ and the libration angle $\theta(t)$ that satisfy the deployment dynamics equations and the following boundary conditions: $l_0 = 0.5\,m$, $\dot{l}_0 = 0\,m/s$, $\theta_0 = 3.4\,rad$, $\dot{\theta}_0 = 0\,rad/s$, $l_f = 3000\,m$, $\dot{l}_f = 0\,m/s$, $\theta_f = \pi\,rad$, $\dot{\theta}_f = 0\,rad/s$. For additional details see [19]. The resulting reference deployment trajectory is shown in Fig. 5. The initial part of this reference trajectory provides the reference profiles for tether deployment velocity that shall be followed by the deployment mechanism.

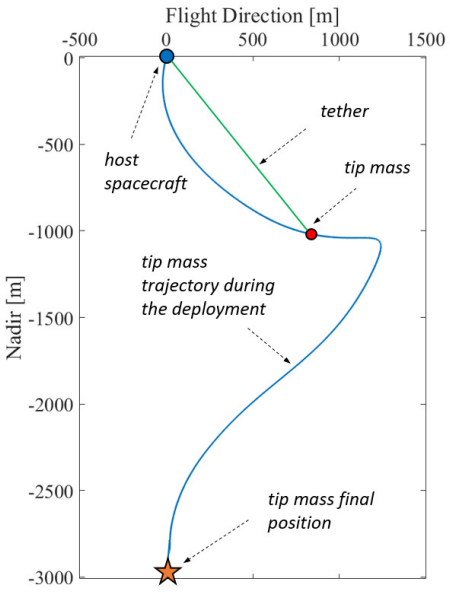

Fig. 5. Deployment trajectory of the tip mass in the orbital plane of the host spacecraft. The x axis is aligned with the radial direction (from the Earth's center to the host spacecraft), the y axis lies on the orbital plane and points toward the Flight Direction (FD) of the host spacecraft.

V. Experimental Results

This section presents the experimental results of a laboratory test that show the verification of the deployment procedure. Specifically, the mock-up was configured to have the following settings: force actuated by each thruster $F_{thr,i} = 0.25\,N$ (all the 6 on-board thrusters are nominally identical), hence $F_{thr} = 0.50\,N$; distance between the thrusters for the attitude control $b = 0.4\,m$; maximum control torque $\tau_{max} = F_{thr,i} \cdot b = 0.1\,Nm$. Moreover, the tip mass moch-up has a total mass $m_{mock-up} = 22\,kg$.

The extracting pulleys were programmed to generate a deployment reference profile in terms of length rate $\dot{l}_{ref}(t)$ with an initial constant-acceleration phase of about $6.3\,mm/s^2$ for the first $14\,s$ of the deployment followed by a constant-velocity phase of about $85\,mm/s$ (see the bottom panel of Fig. 7).

At the beginning of the deployment maneuver the following sequence of operations were carried out in a rapid sequence: (1) start sensors data acquisition, (2) thrust actuation; (3) latching mechanism disengagement, and (4) tether deployment. Figure 6 reports the resulting deployment trajectory of the mock-up reconstructed from the MC system and compared with a trajectory obtained using the same mock-up without the attitude control from a previous test [25]. It is evident that the attitude control system is able to compensate the rotation caused by the reel rotation, resulting in a deployment trajectory that is close to rectilinear.

The actual tether length $l(t)$ and length rate $\dot{l}(t)$ time profiles are shown in Fig. 7, compared with the corresponding reference profiles. As it can be seen, $l(t)$ is very close to $l_{ref}(t)$, meaning that the pulley system is able to correctly follow the precomputed deployment profile (RQ1). There are some oscillation of $\dot{l}(t)$ about $\dot{l}_{ref}(t)$, but this behaviour does not invalidate the tracking of $\dot{l}_{ref}(t)$. Those oscillations are related to spikes in the external tether tension $T_t(t)$, as shown in Fig. 8. The spikes in $T_t(t)$ can be reduced employing an in-line damper in series with the tether and connected to the host spacecraft.

Figure 9 shows the tether tension $T_{t,i}(t)$ measured by the load cell internal to the deployment mechanism, compared to $\dot{l}(t)$ and $\dot{l}_{ref}(t)$. This figure clearly indicates that the profile of $T_{t,i}(t)$ has a shape similar to the $\dot{l}(t)$ profile. In addition, since $T_{t,i}(t)$ is always positive, the tether inside the deployment mechanism is always in tension, and that prevents the tape from becoming tangled inside the deployer.

To conclude, Fig. 10 shows the tether angle $\alpha(t)$, i.e. the angle between the tether direction and the y-axis of the mock-up along which the propulsive force F_{thr} is directed. These results prove the capability of the on-board propulsive subsystem to control the tip mass attitude during the early and critical phase of deployment, by keeping the tether angle $\alpha(t)$ within the desired range $\pm 10\,deg$ (RQ2).

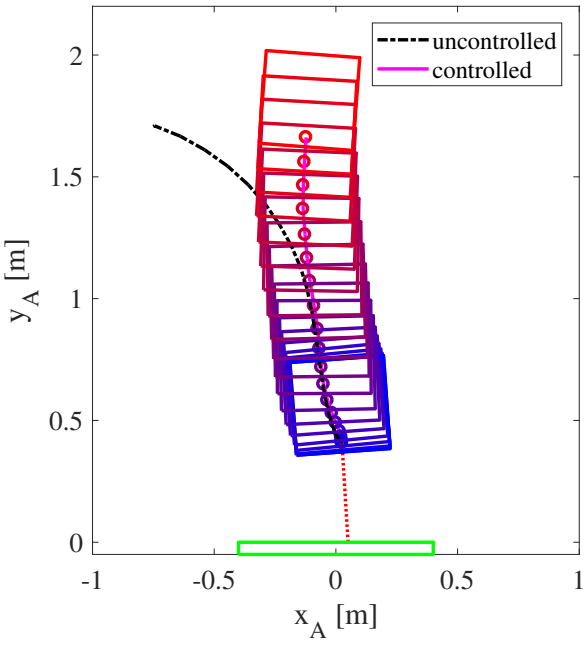

Fig. 6. Deployment trajectory of the mock-up reconstructed by the MC system. The tether exiting point from the mock-up during the deployment is marked with a colored circle; the tether at the beginning of the deployment is depicted with a dashed red line, while the green rectangle represents the host spacecraft. The dashed black line represents the trajectory of the tether exiting point from the mock-up during the deployment in a previous test without attitude control [25].

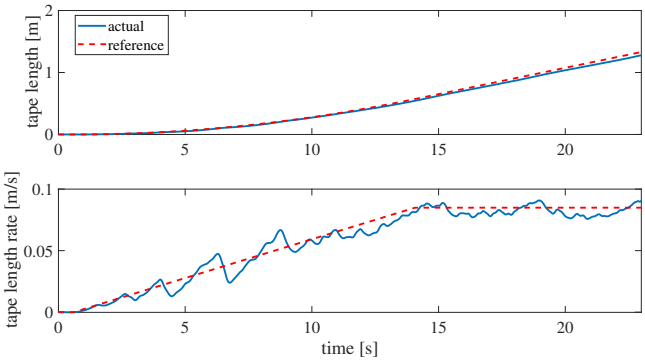

Fig. 7. Tether length (top panel) and tether length rate (bottom panel) time profiles. The reference profiles $l_{ref}(t)$ and $\dot{l}_{ref}(t)$ are marked with a dashed red line and the actual profiles $l_(t)$ and $\dot{l}(t)$ estimated by the Motion Capture are depicted in continuous blue line.

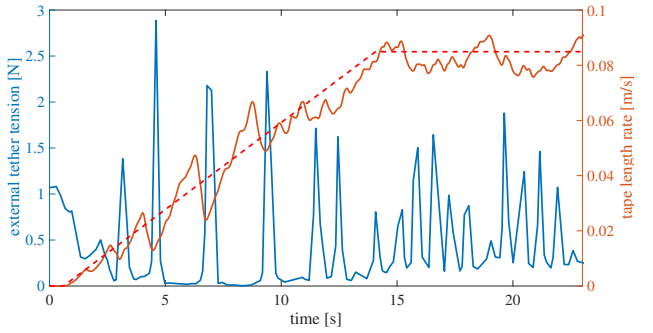

Fig. 8. Tether tension $T_t(t)$ measured by the external load cell, depicted in blue, tether length rate $\dot{l}(t)$, depicted in orange, and the reference profile for the tether length rate $\dot{l}_{ref}(t)$ depicted in dashed red line.

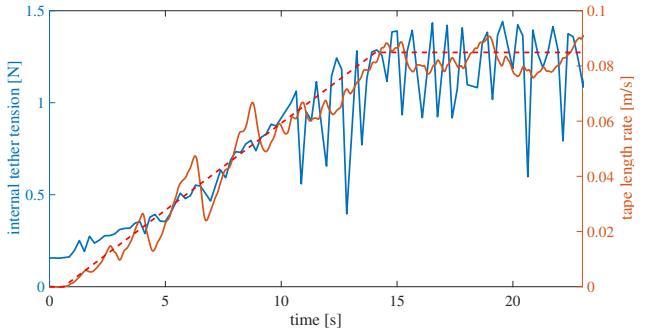

Fig. 9. Tether tension $T_{t,i}(t)$ measured by the load cell internal to the deployment mechanism, depicted in blue, tether length rate $\dot{l}(t)$, depicted in orange, and the reference profile for the tether length rate $\dot{l}_{ref}(t)$ depicted in dashed red line.

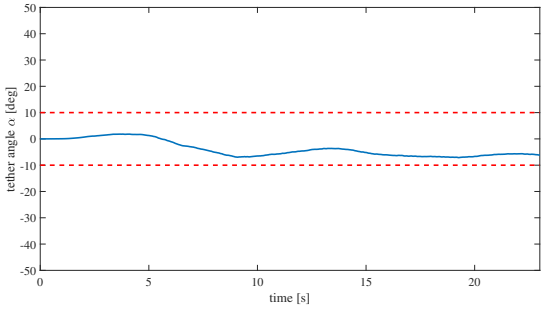

Fig. 10. Time profile of the tether angle α in solid blue line and the upper and lower bounds in dashed red line.

VI. Conclusions

This paper presents the experimental verification of the performance of the deployment mechanism developed in the framework of the H2020 E.T.PACK project. This configuration of the deployment mechanism consists of a tether deployment concept based on a rotating reel and extracting pulleys to deploy the tape-shaped tether, a passive brake applied to the rotating reel to prevent tape entanglements and a sensor based on a beam-type load cell to monitor the tether tension during deployment. The deployment mechanism was integrated into a mock-up equipped with a cold-gas thrust system employed also for the tip-mass attitude control during deployment. The mock-up equipped with the deployment mechanism was tested on the low-friction facility SPARTANS of the University of Padova.

Through a dedicated test campaign we proved: (a) the deployment mechanism capability to follow a prescribed deployment reference profile of the tether length vs time, (b) the effectiveness of the sensor systems to monitoring the tether tension during deployment, both internal to the deployment mechanism and externally, and (c) the validity of the on-board propulsive subsystem in controlling the tip mass attitude

during the early and critical phase of the deployment.

VII. Acknowledgment

This work was supported by the European Commission's H2020 Research and Innovation Program under Grant Agreement No. 828902 (E.T.PACK Project).

References

[1] M. Cartmell and D. McKenzie, "A review of space tether research," *Progress in Aerospace Sciences*, vol. 44, no. 1, pp. 1–21, 2008.

[2] M. L. Cosmo and E. C. Lorenzini, "Tethers in space handbook," 1997.

[3] C. Colombo, A. Rossi, F. Dalla Vedova, *et al.*, "Effects of passive de-orbiting through drag and solar sails and electrodynamic tethers on the space debris environment," in *69th International Astronautical Congress (IAC 2018)*, International Astronautical Federation, IAF, 2018, pp. 1–16.

[4] M. Cartmell and S. Ziegler, "Experimental scale model testing of a motorised momentum exchange propulsion tether," in *37th Joint Propulsion Conference and Exhibit*, 2001, p. 3914.

[5] L. Olivieri, F. Sansone, M. Duzzi, and A. Francesconi, "Ted project: Conjugating technology development and educational activities," *Aerospace*, vol. 6, no. 6, p. 73, 2019.

[6] P. Williams, "Dynamic multibody modeling for tethered space elevators," *Acta Astronautica*, vol. 65, no. 3-4, pp. 399–422, 2009.

[7] M. J. Mashayekhi and A. K. Misra, "Optimization of tether-assisted asteroid deflection," *Journal of Guidance, Control, and Dynamics*, vol. 37, no. 3, pp. 898–906, 2014.

[8] P. Huang and F. Zhang, *Theory and Applications of Multi-Tethers in Space*. Springer, 2020.

[9] Y. Chen, R. Huang, L. He, X. Ren, and B. Zheng, "Dynamical modelling and control of space tethers: A review of space tether research," *Nonlinear Dynamics*, vol. 77, no. 4, pp. 1077–1099, 2014.

[10] R. Mantellato, L. Olivieri, and E. Lorenzini, "Study of dynamical stability of tethered systems during space tug maneuvers," *Acta Astronautica*, vol. 138, pp. 559–569, 2017.

[11] R. Mantellato, A. Valmorbida, and E. Lorenzini, "Thrust-aided librating deployment of tape tethers," *Journal of Spacecraft and Rockets*, vol. 52, no. 5, pp. 1395–1406, 2015.

[12] R. Mantellato, M. Pertile, G. Colombatti, and E. Lorenzini, "Analysis of passive system to damp the libration of electrodynamic tethers for deorbiting," in *AIAA Space 2013 conference and exposition*, 2013, p. 5390.

[13] B. Yu, L. Geng, H. Wen, T. Chen, and D. Jin, "Ground-based experiments of tether deployment subject to an analytical control law," *Acta Astronautica*, vol. 151, pp. 253–259, 2018.

[14] M. Dobrowolny and N. Stone, "A technical overview of tss-1: The first tethered-satellite system mission," *Il Nuovo Cimento C*, vol. 17, no. 1, pp. 1–12, 1994.

[15] C. Bettanini, E. Lorenzini, G. Colombatti, A. Aboudan, and M. Massironi, "Cutie: A cubesats tether-inserted mission for moon exploration," *Acta Astronautica*, vol. 152, pp. 580–587, 2018.

[16] G. Grassi, A. Gloder, L. Pellegrina, *et al.*, "An innovative space tether deployer with retrieval capability: Design and test of star experiment," *Proceedings of the 68th IAC, Adelaide, Australia*, pp. 25–29, 2017.

[17] S. Coffey, J. A. Carroll, P. Oppenheimer, *et al.*, *Separation system and burn wire release mechanism for tethered spacecraft*, US Patent 10,266,284, Apr. 2019.

[18] R. Mantellato, "Investigation of deorbiting systems using passive electrodynamic propulsion," 2015.

[19] G. Sarego, L. Olivieri, A. Valmorbida, *et al.*, "Deployment requirements for deorbiting electrodynamic tether technology," *Proceedings of the Aerospace Europe Conference 2020*, 2020.

[20] A. Valmorbida, M. Mazzucato, S. Tronco, S. Debei, and E. Lorenzini, "SPARTANS - A cooperating spacecraft testbed for autonomous proximity operations experiments," in *Conference Record - IEEE Instrumentation and Measurement Technology Conference*, vol. 2015-July, 2015, ISBN: 9781479961139. DOI: 10.1109/I2MTC.2015.7151360.

[21] A. Valmorbida, M. Mazzucato, S. Tronco, M. Pertile, and E. Lorenzini, "Design of a ground-based facility to reproduce satellite relative motions," in *4th IEEE International Workshop on Metrology for AeroSpace, MetroAeroSpace 2017 - Proceedings*, 2017, ISBN: 9781509042340. DOI: 10.1109/MetroAeroSpace.2017.7999619.

[22] A. Valmorbida, M. Mazzucato, A. Aboudan, and S. Tronco, "Test of attitude control maneuvers with a Satellite Formation Flight testbed," in *2014 IEEE International Workshop on Metrology for Aerospace, MetroAeroSpace 2014 - Proceedings*, 2014, ISBN: 9781479920693. DOI: 10.1109/MetroAeroSpace.2014.6865965.

[23] A. Valmorbida, M. Mazzucato, and M. Pertile, "Calibration procedures of a vision-based system for relative motion estimation between satellites flying in proximity," *Measurement*, p. 107 161, Oct. 2019, ISSN: 02632241. DOI: 10.1016/j.measurement.2019.107161.

[24] I. S. Team Commands, *Bocop: An open source toolbox for optimal control*, http://bocop.org, 2017.

[25] L. Olivieri, A. Valmorbida, G. Sarego, *et al.*, "Test of tethered deorbiting of space debris," *Advances in Astronautics Science and Technology*, vol. 3, no. 2, pp. 115–124, 2020. DOI: https://doi.org/10.1007/s42423-020-00068-9.